APH N.S., Heavy Ion Physics 15/1–2 (2002) 155–171

HEAVY ION PHYSICS
©Akadémiai Kiadó

The Percolation Mechanism for Fragmentation of Nuclei Using Monte Carlo Technique

A. El-Naghy,[1] M. Mohery[2] and Kh.H. Gad[2]

[1] Physics Department, Faculty of Science, Cairo University, Giza, Egypt
[2] Physics Department, Faculty of Science, South Valley University, Sohag, Egypt

Received 14 September 2001

Abstract. A statistical bond-percolation model for the fragmentation has been applied to the proton-induced reactions assuming a lattice structure to the pre-fragment nucleus and using the Monte Carlo technique to determine the bond to be broken. The model succeeded to reproduce the essential features of the mass yield curves for the p–Cu reaction at 3.9 GeV and to describe qualitatively the charge and the multiplicity distributions of the projectile fragments for the ^{28}Si interactions with the quasi-free emulsion nucleon at 3.7 AGeV.

Keywords: Monte Carlo simulations, projectile and target fragmentation, nuclear emulsion
PACS: 24.10.Lx, 25.70.Mn, 29.40.Rg

1. Introduction

Many theoretical models have been proposed to study the multifragmentation processes [1–7]. Among the statistical approaches, the percolation theory postulates that the nucleus is considered as a lattice and the nucleons are distributed over points, which are called lattice sites. Every lattice site represents a nucleon. The occupied sites are either isolated from each other or they form small groups of neighbors called clusters.

There are three types of percolation: the site percolation, the bond percolation and the hybrid or site-bond percolation [8–27]. In the bond percolation [14–19], all sites are occupied but there exists a probability for breaking the bond where the breaking probability P_B increases with increasing the incident energy and decreases with increasing the impact parameter. The excitation energy can be converted into a percolation bond-breaking probability [20, 21] via the relation

1219-7580/02/ $ 5.00

$$P_B = 1 - \frac{2}{\sqrt{\pi}} \Gamma\left(\frac{3}{2}, 0, \frac{E_B}{T}\right) , \quad (1)$$

where Γ is the generalized incomplete gamma function, E_B is the binding energy per nucleon in the residue and T is the temperature [$T = \sqrt{E^*/a}$, where E^* is the excitation energy and a is the level density parameter ($a = A/8$ MeV)].

As the nucleus expands, the available space increases and the nucleons can form clusters which can be more or less extended. The parameter P_B is related to the strength of the bonding between nucleons. For a nucleus with zero thermal excitation energy, $P_B = 1$, increasing E^* decreases the strength of the bonds which vanish completely when E^* equals the binding energy [27]. The percolation has been extensively discussed in Refs [13–18,23–33]. The nuclear lattice model of the proton-induced multifragmentation reactions is discussed in Section 2. A purely statistical model, which implies the bond-percolation mechanism with the minimum physical parameters: the bond breaking and the size of the prefragment nucleus (Section 3) has been applied to study the mass yield distribution of the fragments produced from p–Cu reactions at 3.9 GeV (Section 4). The model has shown to be able to describe qualitatively the charge and the multiplicity distributions of ^{28}Si with the quasi free emulsion at 3.7 AGeV (Sections 5 and 6).

This has been achieved by generating one thousand events for each value of the breaking probability by the Monte Carlo technique. The effect of varying the impact parameter has also been studied. The huge number of simulated events gave an opportunity to study the mass yield distribution and also the dependence of the average multiplicity of the fragments on the breaking probability. Finally, the conclusions are given in Section 7.

2. Nuclear Lattice Model of the Proton-Induced Multi-Fragmentation Reactions

The production of the complex fragments in the nuclear collisions at intermediate and high energies, has received a great interest in nuclear physics. Experiments have been carried out using both proton and heavy-ion beams and the literature is now extensive (for a review, see e.g. Ref. [29]).

The properties of the infinite nuclear matter [34–36] indicate that a "liquid–gas" phase transition is to be expected and that the physical conditions attainable can probe the relevant region of the nuclear equation of state. The calculations for the real, finite nuclei also suggest the presence of phase instability [37–40]. On the other hand, though, investigations of the fragmentation of hot classical drops subjected to classical molecular dynamics [41] suggest that the multifragmentation reactions cannot be used to study the phase diagram in the region of the critical point. Sequential evaporation has been extended to higher excitation energies [4, 42] and has shown to be useful for obtaining some information on the time development of the system. Initially, the system is supposed to be in a state of thermal equilibrium and the evaporation is a surface phenomenon. Different theoretical fragmentation

models based on a droplet description of the nucleus have been proposed [43, 44], and the liquid–gas phase transition has been studied extensively [36, 45]. Power laws in the mass distribution, however, are by no means specific to the liquid–gas phase transitions but can be observed in other fragmenting systems as well as have pointed out Hüfner and Mukhopadhyay [46] stating that

$$\sigma(A_F) \propto A_F^{-\lambda}, \qquad A_F < A_T/3\,, \tag{2}$$

where λ is the exponent. In the inclusive mass yield data for the reactions of p+Kr and p+Xe, at the energies of 80 to 350 GeV [2,5], the value of the exponent λ was found to be $\approx$2.6. Since the mass yield distribution for the droplets condensing at the critical point in a Van der Waals gas follows a similar power law: $\sigma(A) \propto A^{-\tau}$ with a value of $\frac{7}{3}$ for the critical exponent τ, Hirsch et al. [47] suggested that the nuclear multifragmentation proceeds via a liquid–gas phase transition of the nuclear matter. Hüfner and his group have therefore proposed a so-called minimum information model [5] which uses only the charge conservation law and the principle of maximum entropy for its predictions based on statistical calculations. Then, it was refined [48] and extended to include the law of the total energy conservation [49]. To obtain such a method, Bauer proposed the nuclear lattice model [14–16]. In its simplest form, the nucleons are considered to occupy the sites of a three-dimensional simple-cubic lattice. Neighboring pairs of sites are initially connected by bonds. Some bonds are then broken in a model-dependent manner and the size distribution is evaluated for the connected nucleons or "clusters" and identified with nuclei. Such a flexible model allows the study of the effects of the various assumptions. Breaking the bonds in a random, uniform way corresponds to a purely statistical break-up, which may be associated with the multifragmentation of a thermalized system. In the percolation theory, the breaking probability P_B is reasonably assumed to be an increasing function of the excitation energy per nucleon E^* of the target [50].

3. Percolation Model of Nuclear Fragmentation

Percolation models [10] are generally based on two points: the description of the distribution of a set of points in a d-dimensional space and a criterion for deciding if two given points are connected. The connection with the bond percolation theory is established according to the fact that the target nucleons are represented by points occupying a simple cubic three-dimensional lattice in the coordinate space. In general, it would be possible to use any lattice structure.

The lattice spacing l can be computed approximately from the nuclear saturation density $l = 1/\rho_0^{1/3} \approx 1.8$ fm, where ρ_0 is the nucleon density near the center of the nucleus and equals 0.165 fm^{-3}.

The number of points used equals the number of the target nucleons and is conserved during the calculations, therefore automatically satisfying the mass con-

servation law in the fragmentation process

$$\sum_{i=1}^{m} A_F(i) = A_T\,, \tag{3}$$

where $A_F(i)$ is the mass number of the ith fragment and m is the total multiplicity of all the fragments.

The nucleons are connected to their nearest neighbors on the lattice via bonds representing the short-ranged nuclear interactions. The number G of these nearest neighbors in the simple cubic three dimensional lattice is 6, i.e. $G = 6$. These bonds are then broken with a probability P_B, which is the percolation parameter and depends linearly on the excitation energy per nucleon E^* of the target

$$P_B = \frac{E^*}{E_B} = \frac{E^*}{E_{\text{bond}}\, G/2}\,, \tag{4}$$

where E_{bond} is the energy required to break one bond and E_B is the nuclear matter binding energy per nucleon (16 MeV).

No straightforward way exists for calculating the excitation energy E^* as a function of the beam energy. Therefore, P_B will be used as an adjustable parameter to fit the experimental mass yield data. Then, Eq. (4) is used to estimate the total excitation energy deposited in the target. This equation can only be valid for the excitation energies E^* which are smaller than the nuclear matter binding energy E_B [16].

It is interesting to notice the similarity between the Bethe–Weizsäcker description of the nuclear binding energy and the results obtained using the Bauer approach [16]. Using a lattice, one simulates a nucleus with Z protons and $(A - Z)$ neutrons where the sites occupied by the protons are randomly chosen. Each time a proton is adjacent to a neutron, an energy V_1 (and V_2 for the other cases) is attributed to the corresponding bond. Calling N_1 the number of the proton–neutron bonds and N_2 the number of the other bonds, one can define the binding energy per nucleon by [25]

$$E_B = (N_1 V_1 + N_2 V_2 - V_c)/A\,, \tag{5}$$

V_c being the Coulomb energy and A is the mass number of the nucleus given by $A = \frac{4}{3}\pi R^3$, where ρ is the density of the nucleus.

The simulation shows that $V_c \simeq 0.72 Z^2 \times A^{-1/3}$ and that the length scale on the lattice corresponds to a density equal to 0.165 fm^{-3}. An analytical formula for the binding energy per nucleon E_B can be obtained by simply estimating N_1 and N_2.

In a cubic lattice, the total number of bonds between the adjacent sites is equal to $3A(1 - A^{-1/3})$. When the lattice is inscribed in a sphere, the surface term increases and the corresponding total number of bonds can be fitted by the relation: $3A(1 - 1.2A^{-1/3})$, the neutron excess is given by $\mu = (N - Z)/(N + Z)$, the probabilities for a site to be occupied by a proton or a neutron are $P_p =$

$(1-\mu)/2$, $P_n = (1+\mu)/2$, respectively, and the percentage of n–p bonds is $2P_nP_p = (1-\mu^2)/2$. For the other bonds, one gets

$$P_p^2 + P_n^2 = \frac{1+\mu^2}{2}\,. \tag{6}$$

Using the above equations, one obtains

$$\begin{aligned} E_B &= \frac{3}{2}(V_1+V_2) - A^{-1/3}\left(1.2\times\frac{3}{2}(V_1+V_2)\right) - \left(\frac{N-Z}{A}\right)^2\left(\frac{3}{2}(V_1-V_2)\right) \\ &\quad + A^{-1/3}\left(\frac{N-Z}{A}\right)^2\left(1.2\times\frac{3}{2}(V_1-V_2)\right) - 0.72Z^2A^{-4/3}\,. \end{aligned} \tag{7}$$

The first three terms correspond to the volume, surface and asymmetry contributions, respectively and the last one is the Coulomb term.

Using the values $V_1 = 8.5$ MeV and $V_2 = 2$ MeV, one can fairly well reproduce the coefficients of the standard mass formula except for the asymmetry term, which is too low. The fourth term in Eq. (7) (mixing surface and asymmetry) does not appear in the classical mass formula.

Calculating the binding energy per nucleon for Cu, using only the volume and the surface term, yields

$$E_B = 15.75\ \text{MeV} - 17.8\ \text{MeV}\times A^{-1/3} = 11.3\ \text{MeV}\,,$$

the total number of bonds between adjacent sites is equal to $3\times64\,(1-64^{-1/3}) = 144$ bonds, each one represents a binding energy of

$$E_{\text{bond}} = 15.75\ \text{MeV}\times 2/G = 5.25\ \text{MeV}\,. \tag{8}$$

Therefore, one obtains an effective binding energy per nucleon equal to

$$E_B = E_{\text{bond}}\times 144/64 \approx 11.81\ \text{MeV} \tag{9}$$

which is quite close to the previously obtained value.

The breaking probability P_B, given by Eq. (4), has to be dependent on the impact parameter b of the proton and can be calculated according to Bauer [16] by integrating over the nucleon density of the target along the path of the projectile

$$P_B(b) = \frac{P_0\int_{-\infty}^{+\infty}\rho[R(b)]dR}{\int_{-\infty}^{+\infty}\rho[R(0)]dR}\,. \tag{10}$$

For numerical calculations, a standard Woods–Saxon parametrization of the density $\rho(r)$ is used. Thus, P_B is a monotonically falling function of b and $P_B(0) = P_0$. This approach is motivated by the Glauber approximation and will be used to describe the impact parameter dependence of P_B.

For a given $P_B(b)$, one generates a random number ξ_{ijk} between 0 and 1 for every bond B_{ijk} (where the indices correspond to the spatial location of the center of the lattice bond) and decides if the bond will be broken or not,

$$\xi_{ijk} \begin{cases} > P_B \Longrightarrow B_{ijk} & \text{unbroken}, \\ \leq P_B \Longrightarrow B_{ijk} & \text{broken}. \end{cases} \tag{11}$$

This means that using the breaking probability P_B as an input parameter, the Monte Carlo algorithm decides for each bond individually whether it is broken or not. This procedure is followed by a counting algorithm, which looks for clusters and evaluates their sizes. The cluster counting is the most time-consuming part of any percolation-like calculation and the algorithm of [15] is used in the present work. Let us denote the set of all grid points in an $n \times n \times n$ cube by A and by $A^{(0)} \leq A$ the subset of sites occupied by uncounted "nucleons". Note that for each member of A only one flag is required to indicate whether it belongs to $Q = A - A^{(0)}$ or to an already-counted cluster. Initially, bonds are assumed to exist between all neighboring pairs of sites belonging to this subset. These bonds are then "broken" with a probability P_B, and the problem is to "detect" and measure the size of the produced clusters.

One scans A until the first point belonging to $A^{(0)}$ is found. This is denoted by P_1, and one must now find all the other points of $A^{(0)}$ connected by unbroken bonds to P_1. The $C^{(0)} = \{P_1\}$ is called the zeroth generation of C, where $C = \{P_1, \ldots, P_m\}$ represents all the sites of the cluster (of size m), of which P_1 is a member. All sites neighboring P_1 and belonging to $A^{(1)} = A^{(0)} - C^{(0)}$ are then examined and those connected to P_1 by unbroken bonds form $C^{(1)}$. In general the nth generation of C, $C^{(n)}$ consists of all those points of $A^{(n)} = A^{(n-1)} - C^{(n-1)}$ which are connected via bonds to at least one point of $A^{(n-1)}$. This procedure is repeated and the total cluster is then given by $C = \bigcup_{i=0}^{n} C(i)$. Then, a cluster search algorithm is used to find out which nucleons are still connected via bonds and to identify these clusters with the fragments produced by the nuclear collision.

By summing over all the impact parameters and using a large number of Monte Carlo events, one is thus able to generate the mass inclusive mass yield distributions which can be compared to the experimental results.

In an attempt to study the characteristic features of the various physical mechanisms, it is clear that the only input for a given target mass is P_B, for which different prescriptions can be made.

Before considering the experimental data, it is worthwhile exploring the simplest properties of the nuclear lattice model. In order to do it, let us assume that P_B is the same for each bond, independent of its position on the lattice and of the projectile's impact parameter. Using a geometry similar to that used in the nuclear fireball model [51], i.e. assuming that the proton generates a cylindrical fireball in the target, the breaking probability is thus taken to be constant over the spectator nucleons. The obtained results show that the position of the fireball in the target and the number of the nucleons contained in it are irrelevant, provided that only p-induced reactions are considered.

4. Comparison with Data

The behavior of the fragment-mass distributions for the reaction p+Cu with different breaking probabilities from $P_B = 0.35$ to 0.85 has been studied. In Fig. 1, four different intervals are chosen in such a way that for each interval

$$\frac{\pi}{2}\int_{b_{\min}}^{b_{\max}} b\, db = \frac{\sigma_{\text{tot}}}{4} = \frac{\pi R_T^2}{4}, \tag{12}$$

where R_T is the radius of the target nucleus and σ_{tot} is the total cross-section.

Thus, the absolute normalization of the fragment spectra for all intervals are readily comparable. For this reaction, $A_T = 64$ (i.e. $4 \times 4 \times 4$ lattice). From this figure, it can be seen that

a) For small P_B (0.35), corresponding to either a small kinetic energy of the projectile or a high impact parameter, only small fragments are broken off the target nucleus so there are some low-mass fragments, but the major part of the yield lies in particles having a mass similar to that of the target nucleus (residual nucleus). This case is similar to the spallation process.

b) At the intermediate breaking probability P_B (0.60), which corresponds to an intermediate kinetic energy of the projectile or an intermediate impact parameter, a U-shaped mass distribution is obtained showing that the distribution is broad and all kinds of mass numbers are observed.

c) For high P_B (0.74), which corresponds to a high kinetic energy of the projectile or to a small impact parameter, no residual nucleus is present, reflecting a complete break-up of the target.

d) For very high P_B (0.85), corresponding to a very high kinetic energy of the projectile or a very small impact parameter i.e. the collision is very violent, showing a complete disintegration of nuclei into free nucleons and Fig. 1d is monotonically decreasing.

e) Fig. 1e shows a comparison of the present calculations for the mass yield curve with the experimental data of Ref. [52] for the reaction p+Cu at 3.9 GeV beam energy. In inclusive experiments, one is only able to measure the fragment mass distributions that contain contributions from all the impact parameters. Thus, one can only measure an effective exponent λ which is averaged over all the impact parameters. This has also been done for the inclusive results of the present calculations displayed in Fig. 1e.

For the inclusive data, the effective exponent λ is also found to follow a power law. For the present data, using all the fragment masses between 1 and 21 via linear regression the value of λ is found to be 2.406 ± 0.008.

The striking feature of these results is that they show the characteristics that have also been obtained by more complicated theories, in spite of the few assumptions that have been made. In particular, the present model is able to generate

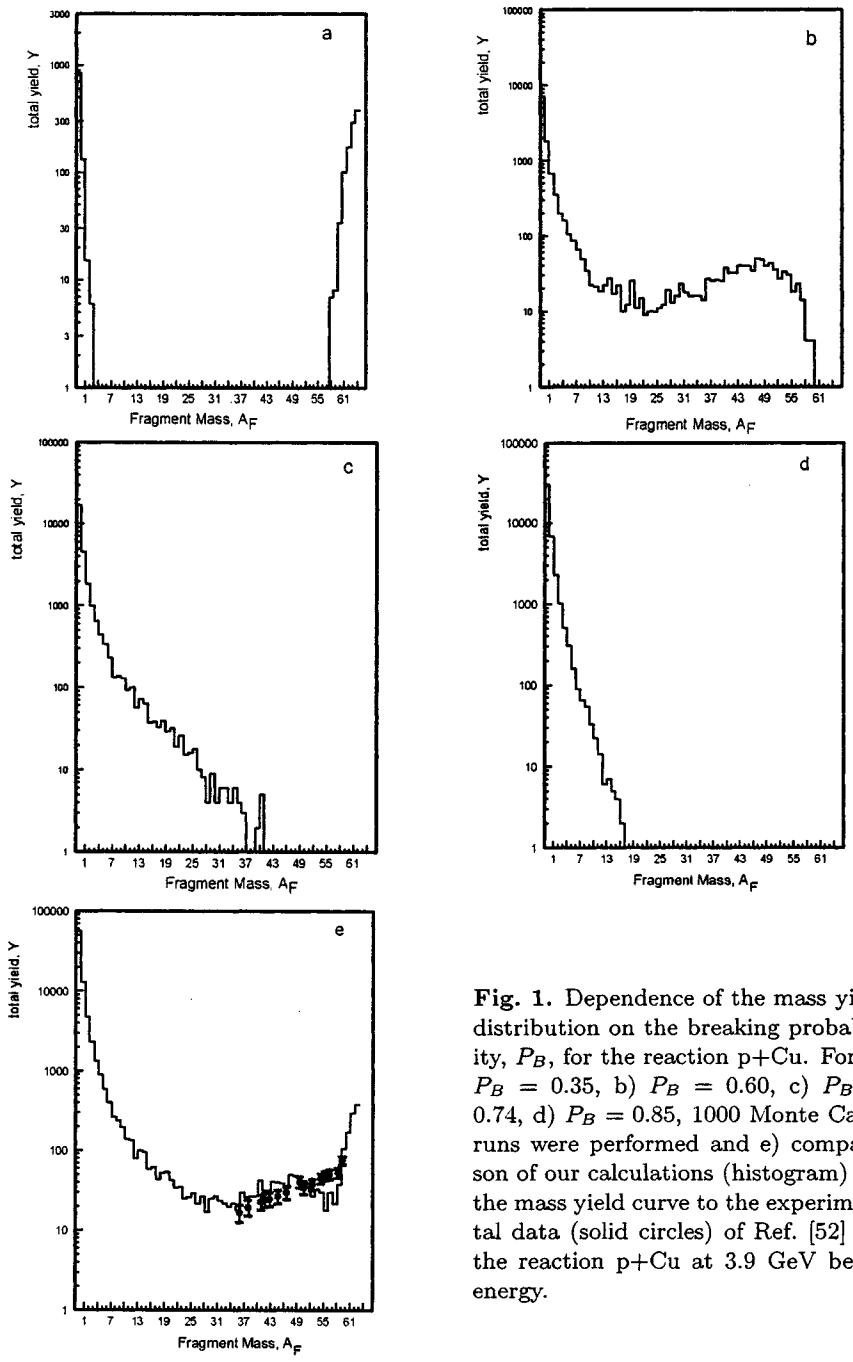

Fig. 1. Dependence of the mass yield distribution on the breaking probability, P_B, for the reaction p+Cu. For a) $P_B = 0.35$, b) $P_B = 0.60$, c) $P_B = 0.74$, d) $P_B = 0.85$, 1000 Monte Carlo runs were performed and e) comparison of our calculations (histogram) for the mass yield curve to the experimental data (solid circles) of Ref. [52] for the reaction p+Cu at 3.9 GeV beam energy.

the U-shape fragment-mass distributions for the intermediate breaking probabilities (Fig. 1b). One can see that the mass yield distributions for the reaction p+Cu show a similar behavior to that of the reactions p+Xe and p+Ag [14–16].

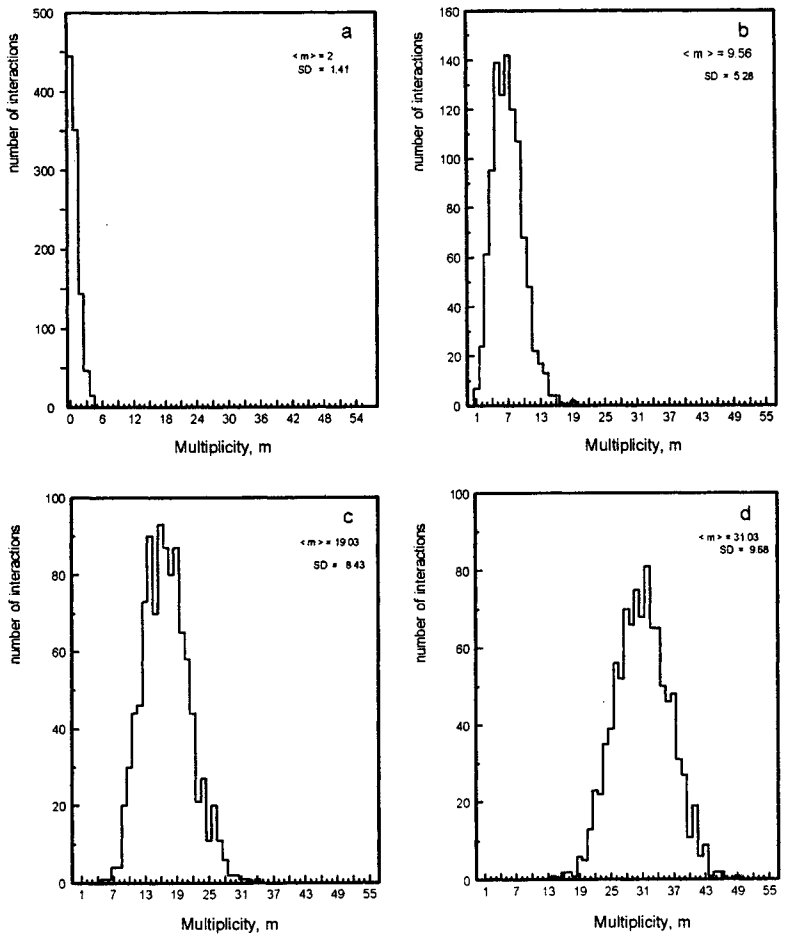

Fig. 2. Multiplicity distribution for the reaction p+Cu at a) $P_B = 0.35$, b) $P_B = 0.60$, c) $P_B = 0.74$ and d) $P_B = 0.85$. Also the mean value $< m >$ and the standard deviation SD of the multiplicity distributions are shown.

Figure 2 displays the dependence of the multiplicity distributions on the breaking probability P_B for the reaction p+Cu, only for $A_F = 1$. It can be seen that the mean fragment multiplicity $< m >$ increases monotonically with the increase of the breaking probability, assumed to be constant over the entire lattice and independent of the impact parameter. This monotonic increase allows the elimination of the somewhat artificial quantity P_B.

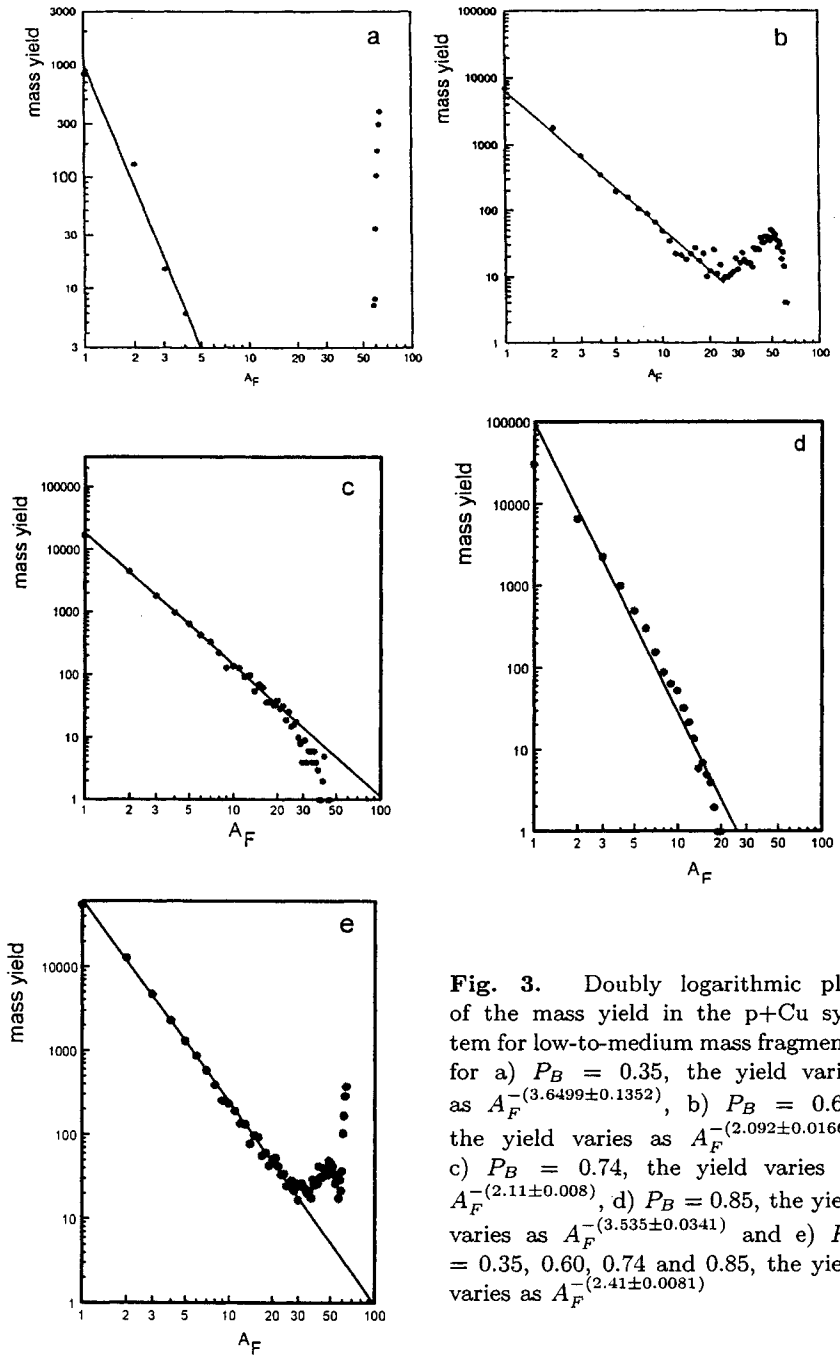

Fig. 3. Doubly logarithmic plot of the mass yield in the p+Cu system for low-to-medium mass fragments for a) P_B = 0.35, the yield varies as $A_F^{-(3.6499\pm0.1352)}$, b) P_B = 0.60, the yield varies as $A_F^{-(2.092\pm0.0166)}$, c) P_B = 0.74, the yield varies as $A_F^{-(2.11\pm0.008)}$, d) P_B = 0.85, the yield varies as $A_F^{-(3.535\pm0.0341)}$ and e) P_B = 0.35, 0.60, 0.74 and 0.85, the yield varies as $A_F^{-(2.41\pm0.0081)}$

Comparison of the experimental data [2,29,47,53–55] with the above-described properties of the nuclear lattice model shows that it allows a qualitative description of the available mass-yield curves.

Mainly, the study of the fragmentation processes has focused on the yield of the medium-mass fragments ($A_F < A_T/3$), for which the data can often be described by a power law, $\sigma(A_F) = \text{const.}\, A_F^{-\lambda}$, then $\ln \sigma(A_F) = \text{const.}\, (-\lambda A_F)$ representing a straight line in a doubly-logarithmic plot whose slope gives the exponent, $-\lambda$. For the copper target nucleus, the power law is only applicable to the fragments having mass numbers between 1 and 21. Figure 3 displays this relation, showing that our results do agree fairly well with the power-law fit showing the validity of the present statistical model.

From Fig. 3, it can be seen that for the low and the intermediate fragment masses, the power law is valid. From the fitting, the exponent λ (i.e. the slope) is found to be equal to 3.650 ± 0.135, 2.092 ± 0.017, 2.110 ± 0.008, 3.535 ± 0.034 and 2.406 ± 0.008 for P_B equals 0.35, 0.6, 0.74, 0.85 and their sum, respectively in a, b, c, d and e.

In the phase-transition model for the fragmentation [45,56], it is expected that this exponent is minimum if the fragmentation occurs at the critical temperature, T_c. Thus $\min(\lambda) = \lambda(T_c) = \tau$, where τ is a critical exponent. A compilation of the experimental data [3] suggests that λ has a minimum at the temperature of almost 12 MeV, which has therefore been identified with T_c.

There has also been an attempt to explain the general behavior of $\lambda(T)$ using purely Coulomb-tunneling effects [57]. The percolation model can be used to calculate λ as a function of P_B. It is clear that there is a minimum at $P_B = 0.60$ $\lambda = 2.092 \pm 0.017$. However, this result is only a consequence of the percolation-like ingredients of this model, and no connection of P_B with a "temperature" has been made.

Figure 4 shows the exponent, λ, as a function of the breaking probability, P_B.

5. Comparison between Nuclear Fragmentation in Collisions of 4.5 A GeV/c ^{28}Si with Quasi-Free Nucleons of Emulsion Nuclei and the Percolation Theory

In high energy nucleus–nucleus collisions, the fragments from the projectile and the target nuclei can be well separated. The process, where a part of the nucleus is suddenly liberated, is called fragmentation [58] and if the second nucleus acts only as an energy injector one denotes it as limiting fragmentation [59]. If the limiting fragmentation is fulfilled and the sources are well separated, in momentum space, the study of the critical behavior by the percolation methods for example becomes useful.

Attempts have been made to study the critical phenomena in nuclear emulsions under the assumption that the projectile fragmentation products can be isolated even in central collisions at 1 AGeV [60] with some positive conclusions concerning

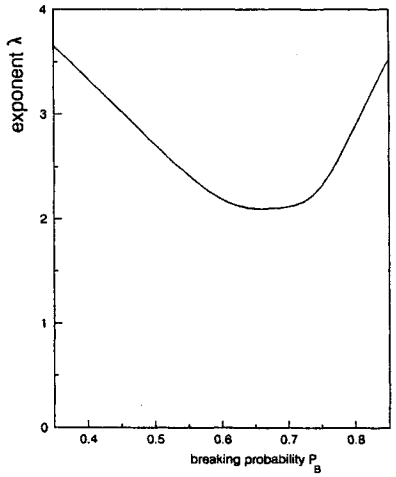

Fig. 4. The exponent, λ, as a function of breaking probability, P_B for the p+Cu system

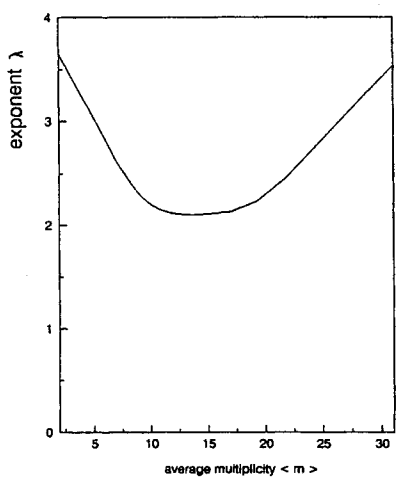

Fig. 5. The exponent, λ, as a function of mean multiplicity, $< m >$, for the p+Cu system

a sharp phase transition [61]. Another attempt done to use the data from the central collisions alone which assumes initial fusion at energies between 20 AMeV and 200 AMeV also indicates the onset of multifragmentation but not as a sharp transition [62].

Percolation theories have been developed to mimic the critical behavior in finite systems [16, 61]. The behavior near criticality has been inferred from the experimentally observed power-law dependence of the intermediate mass fragments ($3 \leq Z \leq 20$) charge distributions [20, 63, 64]. More recently, critical exponents have been extracted from the dependence of the moments of the charge distribution upon some quantities, such as the charge multiplicity, that are typically associated with temperature and/or excitation energy [65].

6. Correspondence between Nuclear Fragmentation and Percolation

Let us discuss the analogy between the nuclear disintegration and the percolation. There is an obvious parallelism between the simple bond percolation and the nuclear disintegration if the excitation energy in an excited nucleus is associated with the number of broken bonds in a percolation simulation. It has been shown [65] that the cross-sections of the total disintegration events should follow a geometrical formula similar to the one suggested by Bradt and Peters [66] for the relativistic (inelastic) nucleus–nucleus interactions,

$$\sigma_{TD} = (1.58A_P^{0.026})^2 \, (A_P^{1/3} + A_T^{1/3} - 0.85A_P^{0.38})^2, \tag{13}$$

where A_P and A_T denote the mass numbers of the colliding nuclei.

To study the ^{28}Si–nucleon (quasi-free nucleon for emulsion) interaction, the ^{28}Si nucleus is considered as a cubic lattice where each nucleon has bonds with its nearest neighbors. Only one parameter, P_B, the probability of the bond breaking, is introduced after setting the dimension of the lattice. For the ^{28}Si, the cubic $3\times3\times3$ lattice is a good approximation.

The number of points used equals the number of the projectile nucleons and is conserved during the calculation, therefore, automatically satisfying the mass conservation law in the fragmentation process

$$\sum_{i=1}^{m} A_F(i) = A_P, \tag{14}$$

where $A_F(i)$ is the mass number of fragment i and m is the total multiplicity of all fragments.

It is interesting to note the similarity between the Bethe–Weizsäcker description of the nuclear binding energy and the result calculated by the present approach. For the ^{28}Si nucleus, calculating the binding energy per nucleon using only the volume and the surface terms of the Bethe–Weizsäcker formula yields

$$E_B = 15.75 \text{ MeV} - 17.8\text{MeV} \times 27^{-1/3} \approx 9.82 \text{ MeV}\,.$$

Representing the ^{28}Si nucleus in a cubic lattice, the total number of bonds between adjacent sites is equal to $3\times27(1-27^{-1/3}) = 54$ bonds, each one represents a binding energy of $E_{\text{bond}} = 15.75$ MeV $\times\, 2/6 = 5.25$ MeV. Therefore, an effective binding energy per nucleon of $E_B = 5.25\times54/27 = 10.50$ MeV is obtained which is quite close to the value obtained above. Therefore, it can be concluded that both approaches give almost the same value of the total binding energy provided that the same Coulomb energy is added when considering the volume and the surface effects only.

Figure 6 shows the charge distribution of $Z \geq 2$ fragments of ^{28}Si in their interactions with a quasi-nucleon type ($n_h = 0, 1$), i.e. only interactions with a hydrogen nucleus or with only one bound nucleon in CNO or AgBr nuclei have been selected and 291 such events have been found for ^{28}Si [67], (chosen out of 1322 ^{28}Si + emulsion interactions at 4.5 AGeV/c, carried out in the laboratory of high energy experimental physics in Cairo University). In the very gentle collisions characterized by $n_h = 0$, the energy transferred to the target nucleus is minimum. In most of these collisions, the projectile nucleus evaporates singly or doubly charged fragments and the residual nucleus is emitted as one big fragment. The charge yield distribution has a U-like shape resulting from the mixture of the characteristic shapes of the spallation and the fission mechanisms.

The best fit curve obtained with the bond percolation model is for $P_B = 0.58$ [18], performing one thousand (1000) Monte Carlo runs. The calculated mass dis-

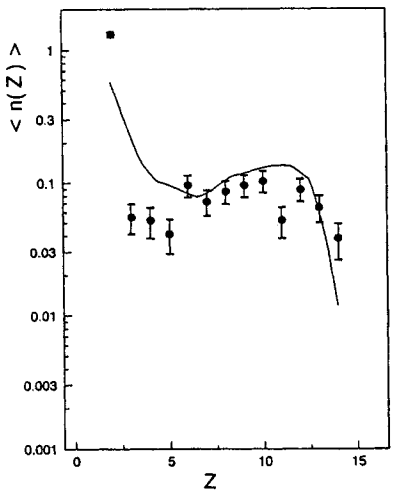

Fig. 6. Charge distribution of the fragments in ^{28}Si interactions with a quasi-nucleon from emulsion ($n_h = 0, 1$). The curve is calculated by the bond percolation model with $P_B = 0.58$.

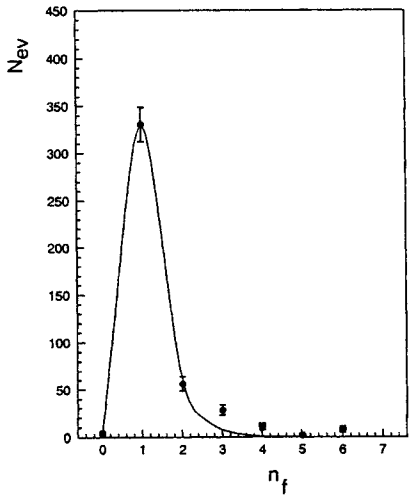

Fig. 7. Multiplicity distribution of the fragments with charge $Z \geq 2$ in interactions of quasi-nucleon type. The curve is calculated by the percolation model and the experimental data [67].

tribution is transformed into a charge distribution by assuming that all $A = 3, 4$ isotopes correspond to $Z = 2$; and all $A = 5, 6$ isotopes correspond to $Z = 3$, etc.

Figure 7 shows the multiplicity distribution for $Z \geq 2$ fragments n_F comparing the experimental data, of the multiplicity distribution of the fragments for ^{28}Si interactions with a quasi-nucleon type, with the curve calculated by the bond percolation model for $P_B = 0.58$, performing 1000 runs. The simulated events gave the best consistency with the experimental data at the breaking probability of 0.58 assuming a cubic lattice $3 \times 3 \times 3$ for the ^{28}Si nucleus.

From Figs 6 and 7, it can be seen that the multiplicity and the charge distributions of the fragments with $Z \geq 6$ are qualitatively described by a statistical percolation model for the quasi-nucleon events where the size of the fragmenting system is well defined. Naturally, no pre-formed alpha-substructures are introduced in the percolation simulation. The alpha emission channel seems however to be stronger than the prediction while the $3 \leq Z \leq 5$ channels are weaker. It has been shown earlier [68] that the ratio between helium (He) and hydrogen fragments decrease as the overlap between the colliding nuclei increases. The cascade evaporation model [68] does not account for the existence of such alpha-structures inside the nuclei and it therefore significantly underestimates the yield of the doubly charged fragments.

7. Conclusions

A statistical model implying the bond-percolation mechanism, with only two physical parameters: the bond breaking probability and the size of the prefragment nucleus, has been studied. This model has successfully reproduced the mass yield distributions for the fragments emitted from the proton–copper reactions at 3.9 GeV. This has been achieved using the Monte Carlo technique by generating one thousand events for each value of the breaking probability. The huge number of simulated events gave an opportunity to study the mass yield distributions and also the dependence of the average multiplicity of the fragments on the breaking probability. The distributions of the charge and the multiplicity for the interactions of ^{28}Si with quasi-free nucleons in emulsion at 4.5 AGeV/c have been compared with the corresponding ones for the events simulated by using the percolation mechanism and using the Monte Carlo technique. The best fit has been obtained, assuming a cubic lattice $3 \times 3 \times 3$ for the ^{28}Si nucleus and at a breaking probability of 0.58.

References

1. J.A. Hauger et al., *Phys. Rev. C* **57** (1998) 764.
2. R.W. Minich et al., *Phys. Lett.* **B118** (1982) 458.
3. J.B. Elliott et al., *Phys. Rev. C* **59** (1999) 550.
4. W.A. Friedman and W.G. Lynch, *Phys. Rev. C* **28** (1983) 950.
5. J. Aichelin, J. Hüfner and R. Ibarra, *Phys. Rev. C* **30** (1984) 107; J. Aichelin and J. Hüfner, *Phys. Lett.* **B136** (1984) 15.
6. X. Campi et al., *Phys. Lett.* **B142** (1984) 8.
7. J.B. Elliott et al., *Phys. Rev. Lett.* **85** (2000) 1194.
8. J.B. Elliott et al., *Phys. Rev. C* **55** (1997) 1319.
9. S.S. Abdel-Aziz, A. El-Naghy and M. Mohery, *26th International Cosmic Rays Conference (ICRC 99)*, Salt Lake City, Utah, 17–25 Aug., HE.1.1.09 (1999) 33.
10. D. Stauffer, *Phys. Rep.* **54** (1979) 1; D. Stauffer, *Introduction to Percolation Theory*, Taylor and Francis, London, 1985.
11. A. Rodrigues et al., *Phys. Lett.* **B458** (1999) 402.
12. C. Cerruti et al., *Nucl. Phys.* **A476** (1988) 74; *Nucl. Phys.* **A492** (1989) 322.
13. O. Knospe, R. Schmidt and H. Schulz, *Phys. Lett.* **B182** (1986) 293.
14. W. Bauer, D.R. Dean, U. Mosel and U. Post, *Phys. Lett.* **B150** (1985) 53.
15. W. Bauer, U. Post, D.R. Dean and U. Mosel, *Nucl. Phys.* **A452** (1986) 699.
16. W. Bauer, *Phys. Rev. C* **38** (1988) 1297.
17. A.J. Cole, et al., *Z. Phys.* **A353** (1995) 279.
18. M.I. Adamovich et al., *Z. Phys.* **A351** (1995) 311.
19. W. Bauer and A. Botvina, *Phys. Rev. C* **52** (1995) 1760.
20. T. Li et al., *Phys. Rev. Lett.* **70** (1993) 1924.
21. T. Li et al., *Phys. Rev. C* **49** (1994) 1630.
22. D.W. Heermann and D. Stauffer, *Z. Phys.* **B44** (1981) 339.

23. J. Németh, M. Barranco, J. Desbois and C. Ngô, *Z. Phys.* **A325** (1986) 347.
24. J. Desbois, Preprint IPNO/TH 86-59 (1986).
25. J. Desbois, R. Boisgard, C. Ngô and J. Németh, *Z. Phys.* **A328** (1987) 101.
26. J. Desbois, *Nucl. Phys.* **A466** (1987) 724.
27. C. Ngô et al., *Nucl. Phys.* **A471** (1987) 381c.
28. S. Redner, *J. Stat. Phys.* **29** (1982) 309.
29. J. Hüfner, *Phys. Rep.* **125** (1985) 129.
30. X. Campi, *J. Phys. A* **19** (1986) L917.
31. H. Ngô et al., *Z. Phys.* **A337** (1990) 81.
32. A.S. Botvina et al., *Yad. Fiz.* **57** (1994) 667.
33. A.S. Botvina et al., *Sov. J. Nucl. Phys.* **57** (1994) 628.
34. G. Saver, H. Chandra and U. Mosel, *Nucl. Phys.* **A264** (1976) 221.
35. H.R. Jaqaman, A.Z. Mekjian and L. Zamick, *Phys. Rev. C* **27** (1983) 2782.
36. A.L. Goodman, J.I. Kapusta and A.Z. Mekjian, *Phys. Rev. C* **30** (1984) 851.
37. H.R. Jaqaman, A.Z. Mekjian and L. Zamick, *Phys. Rev. C* **29** (1984) 2067.
38. P. Bonche, S. Levit and D. Vautherian, *Nucl. Phys.* **A436** (1985) 265.
39. S. Levit and P. Bonche, *Nucl. Phys.* **A437** (1985) 426.
40. D.R. Dean and U. Mosel, *Proc. 23rd Int. Winter Meeting on Nuclear Physics*, Bormio, 1985, p. 798.
41. A. Vicentini et al., *Phys. Rev. C* **31** (1985) 1783.
42. W.A. Friedman and W.G. Lynch, *Phys. Rev. C* **28** (1983) 16.
43. J. Randrup and S.E. Koonin, *Nucl. Phys.* **A356** (1981) 223.
44. D.H.E. Gross, *Nucl. Phys.* **A428** (1984) 313c.
45. M.E. Fischer, *Physics* **3** (1967) 255.
46. J. Hüfner and D. Mukhopadhyay, *Phys. Lett.* **B173** (1986) 373.
47. A.S. Hirsch et al., *Phys. Rev. C* **29** (1984) 508.
48. L.G. Sobotka and L.G. Moretto, *Phys. Rev. C* **31** (1985) 668.
49. L.P. Csernai and J.I. Kapusta, *Phys. Rep.* **131** (1986) 223.
50. W. Bauer, *Proc. 7th High Energy Heavy Ion Study*, GSI Rep., Darmstadt, Oct. 1984.
51. J. Gosset et al., *Phys. Rev. C* **16** (1977) 629; A. Mekjian, *Phys. Rev. C* **17** (1978) 1051.
52. J.B. Cumming et al., *Phys. Rev. C* **10** (1974) 739.
53. G. English, Y.W. Yu and N.T. Porile, *Phys. Rev. C* **10** (1974) 2281.
54. J.R. Grover, *Phys. Rev.* **126** (1962) 1540.
55. S.B. Kaufman et al., *Phys. Rev. C* **14** (1976) 1121.
56. D.K. Scott, *Nucl. Phys.* **A409** (1983) 291c; J.A. Lopez and P.J. Siemens, *Nucl. Phys.* **A431** (1984) 728.
57. D.H. Boal, MSU Preprint MSUCL-443 (1983).
58. A.S. Goldhaber, *Phys. Lett.* **B47** (1974) 306.
59. H.H. Heckman et al., *Phys. Rev. Lett.* **28** (1972) 236.
60. C.J. Waddington and P.S. Freier, *Phys. Rev. C* **31** (1985) 888.
61. X. Campi, *Phys. Lett.* **B208** (1988) 351.
62. B. Jakobsson et al., *Nucl. Phys.* **A509** (1990) 195.

63. J.E. Finn et al., *Phys. Rev. Lett.* **49** (1982) 1321.
64. W. Trautmann, U. Milkau, U. Lynen and J. Pochodzalla, *Z. Phys.* **A344** (1993) 447.
65. V.L. Bogdanov et al., *Yad. Fiz.* **47** (1988) 1841.
66. H.L. Bradt and B. Peters, *Phys. Rev.* **77** (1950) 54.
67. A. El-Naghy et al., *Tr. J. Phys.* **19** (1995) 1.
68. A. El-Naghy et al., *J. Phys. G* **14** (1988) 1125.